

Decay of Entanglement for Solid-State Qubits

F. Bodoky,¹ O. Gühne,^{2,3} and M. Blaauboer¹

¹*Kavli Institute of Nanoscience, Delft University of Technology, Lorentzweg 1, 2628 CJ Delft, The Netherlands*

²*Institut für Quantenoptik und Quanteninformatik,*

Österreichische Akademie der Wissenschaften, 6020 Innsbruck, Austria,

³*Institut für Theoretische Physik, Universität Innsbruck, Technikerstraße 25, 6020 Innsbruck, Austria*

(Dated: March 16, 2019)

We investigate the time evolution of entanglement in solid-state nanosystems using a phenomenological model with local relaxation and dephasing rates. We introduce a class of witness operators (the so-called filtered entanglement witnesses) and use them to predict how long the entanglement of different initially entangled states can realistically be detected. Our model applies to arrays of solid-state qubits, for example electron spin qubits in quantum dots or superconducting flux qubits. By comparing the time required for detection with the time required for generation and manipulation of entanglement, we estimate for a range of different entangled states how many qubits can be entangled in a one-dimensional array of electron spin qubits.

PACS numbers: 03.65.Ud, 03.67.Mn, 73.21.La

I. INTRODUCTION

Entanglement refers to non-classical correlations between two^{1,2,3,4} or more⁵ quantum particles, and the creation of multiparticle entangled states constitutes a key step towards quantum computation⁶. In this work, we investigate the evolution of entangled states under a heuristic decoherence model that is applicable for solid-state qubits. We investigate how and how long the entanglement can be detected, and estimate what kind of entanglement in systems of what size is realistic to generate with actual experimental means and currently known decoherence times.

We consider decoherence of a *local* nature, *i.e.* the qubits decohere in an uncorrelated way, as is the case in solid-state nanosystems such as electron spin qubits in quantum dots⁷, various superconducting qubits⁸ and other solid-state implementations⁹. In these systems, the decoherence can be characterized using a phenomenological model, where each qubit decays on two time scales¹⁰: a relaxation time T_1 and a dephasing time T_2 . The microscopic details of the decoherence are still a matter of intensive research; as an example, we discuss in some detail the state of this research for electron spin qubits in quantum dots, and use the values T_1 and T_2 for this type of solid-state qubits to illustrate our results.

Our proposed means to analyze entanglement are so-called witness operators:^{11,12,13,14,15} locally decomposable observables with a positive expectation value for all separable states, and a negative expectation value for at least one entangled state. The advantage of entanglement witnesses over other methods such as *e.g.* full state tomography is that they require less measurements, and thus less experimental effort to detect and prove the existence of entanglement for a given (mixed) state. Witnesses have intensively been used in experiments with photons^{16,17} and trapped ions¹⁸, but so far only few theoretical proposals exist for using witness operators in solid-state nanosystems¹⁹.

This paper is organized as follows: in Sec. II we briefly summarize the mechanisms influencing the time scales T_1 and T_2 for electron spin qubits. We then introduce the heuristic decoherence model and show how we calculate the decoherence of a multipartite state of separated qubits using the Lindblad formalism. Next (Sec. III) we demonstrate our main ideas and methods using the simple case of two qubits, and introduce the new filtered witness operator. In Sec. IV we consider both GHZ- and W-states for three qubits. In Sec. V we do the same for four qubits and consider in addition the cluster and Dicke entanglement classes. We also discuss the dependence of the decay of entanglement on the initial state. Finally, in Sec VI, we discuss the case of N qubits: We show that the entanglement of a specific GHZ-state can in principle be detected for any finite time, and discuss the feasibility of generating and detecting many-qubit entangled states of electron spin qubits based on decoherence and operation time scales that have been measured in recent experiments on single and double quantum dots.

II. DECOHERENCE MODEL

Physically, decoherence is caused by uncontrolled interactions between the qubit and the environment²⁰. The effects are usually characterized by two time scales, the phase randomization time T_2 (“dephasing time”) and the time T_1 in which the excited state $|1\rangle$ relaxes to the ground state $|0\rangle$ by energy exchange with the environment (“relaxation time”)¹⁰. Below we start with a short review of the quantum-mechanical processes causing decoherence of electron spin qubits in quantum dots, in order to illustrate the microscopic origin behind the T_1 and T_2 times for a particular kind of solid-state qubits. Our heuristic description, however, is entirely based on T_1 and T_2 times and thereby applicable to all types of solid-state qubits that are subject to local decoherence

of individual qubits.

The original idea by Loss and DiVincenzo²¹ proposed to confine single electrons in a quantum dot (an island of charge in a two-dimensional electron gas) and apply a magnetic field to split the degeneracy of the spin-up and spin-down states, thus creating a two-level system serving as carrier for quantum information: an electron spin qubit. Two such qubits interact via a Heisenberg coupling, and this interaction can be controlled by tuning the potential between two neighboring dots. In quantum dots, interactions with the environment are mainly mediated by two processes, spin-orbit interaction and hyperfine interaction⁷.

Let us turn our attention to the spin-orbit interaction first. Spin-orbit interaction is caused by the charge configuration a moving electron feels, and in conventional two-dimensional electron gases there are two contributions, the so-called Dresselhaus²² and Rashba²³ effects, connecting the electron's momentum with its spin. In quantum dots, however, electrons are too strongly confined and thus their momentum is too small to cause changes in their spin: hence the spin-orbit interaction does not directly influence the spin states, but it couples states with different spin and orbital angular momentum²⁴ and thus the effective eigenstates are admixtures of spin and orbital states²⁵. These effective states couple to electric fields, which can then lead to spin relaxation. The main electric field fluctuations are caused by phonons deforming the crystal structure and thus the background field. The relaxation time T_1 due to spin-orbit interaction and phonons can be calculated as a function of the externally applied Zeeman field B_0 ²⁵. This relaxation inevitably leads to dephasing of the qubit state, which by definition has to fulfill $T_2 \leq 2T_1$ (otherwise the density matrix would not be positive definite at all times). When considering spin-orbit interaction only²⁶, we have in fact $T_2 = 2T_1$.

If the atoms of the semiconductor have a non-zero nuclear magnetic moment (as for example in GaAs; in other materials, such as purified SiC, this effect is not present), then the electron spin \vec{S} interacts with the nuclear spins via the hyperfine interaction²⁷, $H_{hf} = \sum_k^N A_k \vec{I}_k \vec{S}$, where N is the number of nuclei whose wave function overlaps with the electron's wave function ($N \approx 10^6$ for typical dots), A_k denotes the coupling strength between the k -th nucleus and the electron and \vec{I}_k is the spin of the k -th nucleus. For an intuitive semiclassical description the effect of the nuclear spins can be treated as an additional magnetic field – the Overhauser field – by replacing $\sum_k^N A_k \vec{I}_k = g^* \mu_B \vec{B}_N$, with g^* the effective g-factor of the electron ($g^* = -0.44$ in GaAs) and the Bohr magneton μ_B . The maximum value this field can reach for GaAs is about²⁸ $B_{max} = 5$ T, if the nuclei are fully polarized. In low magnetic field, the Overhauser field undergoes Gaussian fluctuations around a root-mean-square value^{29,30,31} of (B_{max}/\sqrt{N}) T. The electron thus feels a total magnetic field which consists of the sum of the controlled external field \vec{B}_0 and the random Overhauser field \vec{B}_N .

Let us now first consider the effect of hyperfine interaction on the relaxation time T_1 : With almost no external field B_0 , the relaxation is dominated by flip-flop processes, where a nucleus flops as the electron flips³¹. For stronger B_0 , the energy mismatch between nuclear and electron spin states grows, and energy has to be absorbed by phonons (where the coupling is mediated by both hyperfine and spin-orbit interaction), which becomes more efficient as the field increases and the phonon wavelength becomes closer to the dot size. Thus, T_1 decreases as B_0 increases and measured values range from 170 ms (at $B_0 = 1.75$ T) to 120 μ s ($B_0 = 14$ T)^{32,33}.

As to the effect of the nuclear field on the phase, the field's longitudinal component B_{nuc}^z (parallel to \vec{B}_0) changes the precession frequency of the electron spin by $g^* \mu_B B_{nuc}^z$. The transverse part $B_{nuc}^{x,y}$ changes the precession direction by $\approx g^* \mu_B B_{nuc}^2 / B_0$. This nuclear magnetic field is not only random, but changes in time: two nuclei with different coupling strength A_k can exchange their spin, thus leading to a change in the Overhauser field B_N ; these fluctuations appear on a time scale of 10 – 100 μ s (for a weak external field)³⁴, but could probably be extended up to well more than several seconds to minutes (for the longitudinal nuclear field B_{nuc}^z in a strong external field B_0)³⁵. The bulk dephasing time T_2^* at which the fluctuating nuclear magnetic field removes the phase information can be measured by rotating the spin in the xy -plane, let it evolve freely, and then rotate it back along the z -axis for measurement (so-called spin echo measurements). Each data point then has to be averaged over many measurements, during which the nuclear field evolves. This leads to an average dephasing time T_2^* , which has been measured to be about $\gtrsim 10$ ms³⁶, in agreement with theory³⁰.

The dephasing time T_2 of a single electron, on the other hand, has not been measured yet. Measuring T_2 is hard, since it is not possible to measure the initial orientation and strength of the nuclear field with sufficient precision. Estimates in various regimes predict $T_2 \sim 1 - 100$ μ s: a good way to estimate T_2 is by using a Hahn echo technique, where the free evolution of the spin due to the initial magnetic field is undone by reversing the spin, but not the dephasing due to the change of this nuclear field³⁷. Assuming Gaussian fluctuations of the nuclear field on a time scale of 10 s and $T_2^* = 10$ ns, a time $T_2 = 10$ μ s can be extracted⁷.

We now use the T_1 and T_2 times as the basis for constructing a differential equation for the time evolution of the density matrix of a single qubit in the rotating frame of the external magnetic field. This results in:

$$\frac{d\rho}{dt} = \begin{bmatrix} (1/T_1) \rho_{22} & -(1/T_2) \rho_{12} \\ -(1/T_2) \rho_{21} & -(1/T_1) \rho_{22} \end{bmatrix}. \quad (1)$$

Qualitatively, the off-diagonal phase components decrease at a rate $1/T_2$, and the ground state ρ_{11} gets populated at the expense of the excited state ρ_{22} , where the normalization condition ($\text{Tr}[\rho(t)] = 1$) has to be fulfilled at any time t .

Eq. (1) can be rewritten in the Lindblad formalism³⁸ using the Lindblad operator \mathcal{L} :

$$\begin{aligned} \mathcal{L}\rho = & \frac{\Gamma_1}{2} (2\sigma_+\rho\sigma_- - \sigma_-\sigma_+\rho - \rho\sigma_-\sigma_+) \\ & + \frac{\Gamma_2}{2} (2\sigma_s\rho\sigma_s - \sigma_s\sigma_s\rho - \rho\sigma_s\sigma_s). \end{aligned} \quad (2)$$

Here, $\sigma_{\pm} = 1/2(\sigma_x \pm i\sigma_y)$ and $\sigma_s = \sigma_-\sigma_+$ are products of the Pauli matrices. By comparison of the density matrices resulting from Eqs. (1) and (2), we can identify $\Gamma_1 = 1/T_1$ and $\Gamma_1 + \Gamma_2 = 2/T_2$. The time evolution of a single qubit is then found by solving $\mathcal{L}\rho(t) = d\rho/dt$.

To extend Eq. (2) to multipartite states, we write the Lindblad operator for the k -th qubit as $\mathcal{L}_k = \mathbb{1} \otimes \dots \otimes \mathbb{1} \otimes \mathcal{L} \otimes \mathbb{1} \otimes \dots \otimes \mathbb{1}$, where \mathcal{L} is the k -th operator of a total of N ³⁹. The time evolution of the total N -partite state is then given by solving as before $\mathcal{L}_N\rho(t) = d\rho/dt$, with $\mathcal{L}_N = \sum_{k=1}^N \mathcal{L}_k$. By using this definition we implicitly assumed that the decoherence of each qubit is governed by the same Γ_1 and Γ_2 .

III. TWO QUBITS

Let us first explain our methods and definitions for the simple case of two qubits. A *separable state* ρ_s is defined as a state which can be written as a convex combination of product states^{1,2,4}

$$\rho_s = \sum_i p_i \rho_i^A \otimes \rho_i^B, \quad (3)$$

where ρ^A and ρ^B are states in different subsystems A and B and the probabilities p_i have to fulfill the normalization condition $\sum_i p_i = 1$. If a state is not of this form, it is called *entangled*.

We use witness operators^{11,12,13,14,15} to investigate the entanglement for various states. An observable \mathcal{W} is called an *entanglement witness* if it fulfills the following two requirements:

1. For any separable state ρ_s , the expectation value of \mathcal{W} is larger than zero:
 $\text{Tr}[\mathcal{W}\rho_s] \equiv \langle \mathcal{W} \rangle_{\rho_s} \geq 0 \quad \forall \rho_s \text{ separable.}$
2. There must be at least one entangled state ρ_e for which \mathcal{W} has a negative expectation value:
 $\exists \rho_e \text{ entangled} : \langle \mathcal{W} \rangle_{\rho_e} < 0.$

Therefore, a measured negative expectation value of the witness guarantees that the state is entangled. For the experimental implementation, entanglement witnesses can be decomposed into local measurements (see also below), and they usually require much fewer measurements than procedures such as full state tomography. Thus they are experimentally easier to implement. Finally, it should be noted that witnesses can be used to quantify entanglement, by giving lower bounds on entanglement measures⁴⁰.

The witnesses we use in this paper are derived from the so-called projector-like witness¹⁶:

$$\mathcal{W}_{\psi} = c\mathbb{1} - |\psi\rangle\langle\psi|, \quad (4)$$

with the constant c standing for the maximum overlap between the state $|\psi\rangle$ and any separable state. Physically, this witness encodes the fact that if a state ρ has a fidelity $F = \text{Tr}[\rho|\psi\rangle\langle\psi|]$ larger than c , then ρ must be entangled.

We illustrate our methods for the case of two qubits. We first investigate the time evolution of the Bell state^{1,3} $|\Psi^{-}\rangle \equiv \frac{1}{\sqrt{2}}(|01\rangle - |10\rangle)$. The choice of this Bell-state, the singlet state, is motivated by the fact that it is the ground state of the quantum system consisting of two electron spins in a double quantum dot⁷, thus it is the simplest entangled state that can be created in quantum dots. Along the lines of Eqs. (1) and (2), we can calculate the time evolution of the singlet state as

$$\rho_{\Psi^{-}}(t) = \frac{1}{2} \begin{bmatrix} 2[1 - \alpha(t)] & 0 & 0 & 0 \\ 0 & \alpha(t) & -\beta(t) & 0 \\ 0 & -\beta(t) & \alpha(t) & 0 \\ 0 & 0 & 0 & 0 \end{bmatrix}, \quad (5)$$

with the factors $\alpha(t) = \exp[-t/T_1] \equiv \exp[-\Gamma_1 t]$ for relaxation and $\beta(t) = \exp[-2t/T_2] \equiv \exp[-(\Gamma_1 + \Gamma_2)t]$ for dephasing. With that, the fidelity⁶ $F = \text{Tr}[|\Psi^{-}\rangle\langle\Psi^{-}| \rho_{\Psi^{-}}(t)]$ is given by

$$F(t) = \frac{1}{2} [\alpha(t) + \beta(t)], \quad (6)$$

and the expectation value of the projective witness for $|\Psi^{-}\rangle$ is then calculated using Eq. (4). We find that the maximal overlap is $c = 1/2$ when applied to the decohering state $\rho_{\Psi^{-}}$ from Eq. (5), and

$$\text{Tr}[\mathcal{W}_S \rho_{\Psi^{-}}(t)] \equiv \langle \mathcal{W}_S \rangle_{\Psi^{-}(t)} = \frac{1}{2} [1 - \alpha(t) - \beta(t)], \quad (7)$$

where \mathcal{W}_S is the witness for the singlet state, $\mathcal{W}_S = \mathbb{1} - |\Psi^{-}\rangle\langle\Psi^{-}|$. Analyzing this witness, we see immediately that it becomes positive (and hence does not detect the entanglement any more) after some finite time, though it can be shown (by virtue of the PPT-criterion⁴¹, for example) that the state $\rho_{\Psi^{-}}(t)$ is entangled for any $t < \infty$.

Therefore, our goal is to construct a witness operator which is able to detect the entanglement in the state $\rho_{\Psi^{-}}(t)$ at any time. This can be achieved by a so-called filter operator \mathcal{F} ,

$$\mathcal{F} = \mathcal{F}_1 \otimes \mathcal{F}_2, \quad (8)$$

where the \mathcal{F}_i are arbitrary invertible matrices acting on individual qubits. Since \mathcal{F} is local, application of such a filter operator on a state ρ does not change its entanglement properties, i.e. ρ is entangled, iff $\mathcal{F}^{\dagger}\rho\mathcal{F}$ is entangled.

Equivalently, one can apply filter operators to witness operators \mathcal{W} , and the resulting 'filtered witness operator' $\mathcal{W}^{\mathcal{F}}$ is then given by

$$\mathcal{W}^{\mathcal{F}} = \mathcal{F}\mathcal{W}\mathcal{F}^\dagger. \quad (9)$$

As normalization, we choose $\text{Tr}[\mathcal{W}] = \text{Tr}[\mathcal{W}^{\mathcal{F}}]$, to make the witnesses' mean values comparable.

Our goal is now to design the filter \mathcal{F}_i such that it increases the negativity of the witness, i.e. it should increase the weight of the terms α and β in Eq. (7), so that the filtered witness can be used to detect entanglement during longer times. This can be achieved by the following filter:

$$\mathcal{F}_i = \begin{bmatrix} 1 & 0 \\ 0 & y \end{bmatrix}, \quad (10)$$

with y a positive real number. The normalized filtered witness for the singlet state then takes the form

$$\begin{aligned} \mathcal{W}_S^{\mathcal{F}} &= (\mathcal{F}_1 \otimes \mathcal{F}_2) \mathcal{W}_S (\mathcal{F}_1 \otimes \mathcal{F}_2)^\dagger \\ &= \frac{1}{1+y^4} \begin{bmatrix} 1 & 0 & 0 & 0 \\ 0 & 0 & y^2 & 0 \\ 0 & y^2 & 0 & 0 \\ 0 & 0 & 0 & y^4 \end{bmatrix}. \end{aligned} \quad (11)$$

and the expectation value is given by

$$\langle \mathcal{W}_S^{\mathcal{F}} \rangle_{\Psi^-(t)} = \frac{1}{1+y^4} [1 - \alpha(t) - y^2\beta(t)]. \quad (12)$$

Clearly, $\langle \mathcal{W}_S^{\mathcal{F}} \rangle_{\Psi^-(t)}$ is negative if y is chosen large enough and $t < \infty$ (thus $\beta(t) > 0$). The remaining entanglement (which is not detected by \mathcal{W} , Eq. (7)) in the decohering state can then be detected by measuring this filtered witness operator. The effectiveness of the filter operator crucially depends on the choice of the singlet state $|\Psi^-\rangle$ as the initial state: it can easily be shown that for the other Bell states $|\Phi^\pm\rangle = \frac{1}{\sqrt{2}}(|00\rangle \pm |11\rangle)$ the filtered witness does not detect the entanglement at any time. The decay of entanglement in our model thus strongly depends on the initial state, even within the same basis.

For the experimental implementation, the witness $\mathcal{W}_S^{\mathcal{F}}$ can be decomposed into single-qubit measurements¹⁵:

$$\begin{aligned} \mathcal{W}_S^{\mathcal{F}} &= \frac{1}{4(1+y^4)} [(1+y^4)(\mathbb{1} \otimes \mathbb{1} + \sigma_z \otimes \sigma_z) \\ &\quad - (1-y^4)(\sigma_z \otimes \mathbb{1} + \mathbb{1} \otimes \sigma_z) + 2y^2(\sigma_x \otimes \sigma_x + \sigma_y \otimes \sigma_y)]. \end{aligned} \quad (13)$$

This decomposition requires three measurement settings (namely $\sigma_i \otimes \sigma_i$ with $i \in \{x, y, z\}$) instead of the nine settings full state tomography would require^{14,42}. Similar decompositions exist for all other witnesses occurring in this paper^{16,43}.

In Fig. 1, the evolution of the witness expectation values of both the regular witness Eq. (7) and the filtered witness Eq. (12) are plotted for $\Gamma_1 = 10^3 s^{-1}$, and

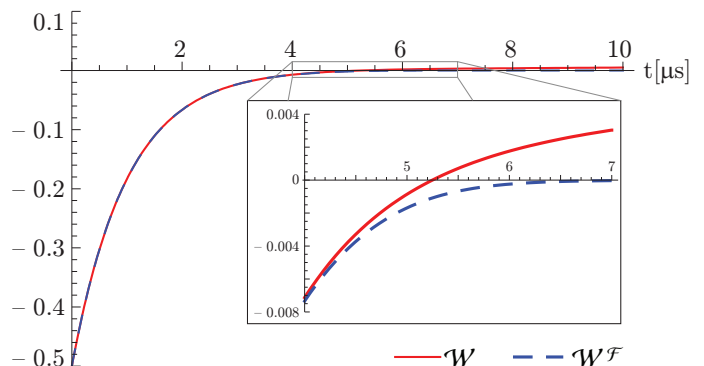


FIG. 1: Expectation values for the regular (Eq. (7), solid red line) and the filtered (Eq. (12), dashed blue line) witness, for $\Gamma_1 = 10^3 s^{-1}$ and $\Gamma_2 = 10^6 s^{-1}$. The inset shows a zoom into the region where the regular witness becomes positive. y is chosen such that the witness expectation value becomes minimized at any given time, thus it is time-dependent.

$\Gamma_2 = 10^6 s^{-1}$. In this limit ($\Gamma_2 \gg \Gamma_1$), the experimental advantage of the filter operator does not manifest itself as strongly as would be the case for $\Gamma_2 \simeq \Gamma_1$; however, the principle advantage that the entanglement can be detected for any finite time is demonstrated in the inset by a zoom into the region where the unfiltered witness becomes positive. The filtered witness remains negative, albeit with a small absolute value, for any finite time.

From this curve, one can conclude that it becomes difficult to detect entanglement under realistic conditions after more than a few μs (depending on the size of the error bars in a given experiment). Consequently, any generation scheme for the Bell states which requires a generation time longer than this time will probably not work in practice.

IV. THREE QUBITS

For three or more particles, the situation is more complicated, since different classes of multiparticle entanglement exist^{44,45,46}.

Let us first discuss the notion of partial separability. A state can be *partially separable*, meaning that some of the qubit states are separable, but not all. An example for three particles is the state

$$|\psi^{bs}\rangle = |\phi^{AB}\rangle \otimes |\phi^C\rangle, \quad (14)$$

where $|\phi^{AB}\rangle$ is a (possibly entangled) state of two qubits (defined on subsystems A and B), and $|\phi^C\rangle$ a state of the third qubit (defined on subsystem C). The state $|\psi^{bs}\rangle$ is separable with respect to a certain bipartite split, so it is called biseparable. A mixed state is biseparable, if it can be written as mixture of biseparable pure states.

If a state is not biseparable, it is genuinely multipartite entangled. There exist different classes of multipartite entangled states⁴⁴ and the number of entanglement

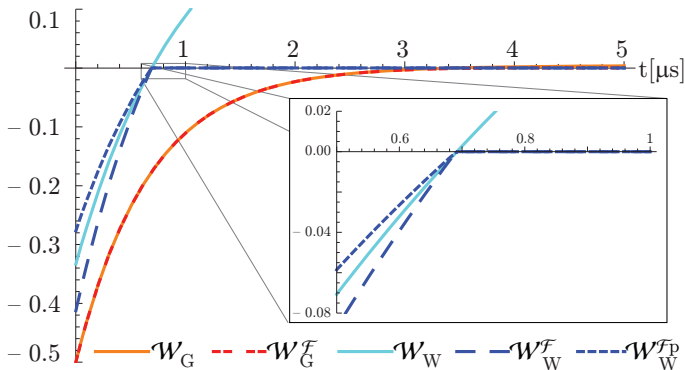


FIG. 2: Expectation values for the witnesses for the tripartite GHZ- and W-states, both regular (solid lines) and filtered (dashed). The projected filter $\mathcal{W}_W^{\mathcal{F}p}$ (see text) is plotted as well, though it is not better than the filtered witness $\mathcal{W}_W^{\mathcal{F}}$. Parameters used are $\Gamma_1 = 10^3 \text{ s}^{-1}$ and $\Gamma_2 = 10^6 \text{ s}^{-1}$. As in Fig. 1, y is chosen so as to minimize the witness expectation value.

classes increases with the number of qubits⁴⁷. An entanglement class can be defined by the following question: given a single copy of two pure states $|\psi\rangle$ and $|\phi\rangle$, is it possible, at least in principle, to transform $|\psi\rangle$ into $|\phi\rangle$ (and vice versa) using local transformations only? Even if the probability of success is small? For three qubits, for example, two entanglement classes exist, the GHZ and the W-class. Every genuine multipartite entangled three-qubit state can be transformed into one of the two states⁴⁴

$$|GHZ_3\rangle = \frac{1}{\sqrt{2}} (|010\rangle + |101\rangle), \quad (15)$$

$$|W_3\rangle = \frac{1}{\sqrt{3}} (|100\rangle + |010\rangle + |001\rangle), \quad (16)$$

$$\langle \mathcal{W}_G^{\mathcal{F}} \rangle_{eG(t)} = \frac{3}{2(1 + 2y^2 + 2y^4 + y^6)} \left(2 + (-3 + 2y^2)e^{-\Gamma_1 t} + (1 - 2y^2)e^{-2\Gamma_1 t} - 2y^3 e^{-\frac{3}{2}(\Gamma_1 + \Gamma_2)t} \right), \quad (19)$$

$$\langle \mathcal{W}_W^{\mathcal{F}} \rangle_{eW(t)} = \frac{13}{3(2 + 3y^2 + 6y^4 + 2y^6)} \left(2 + (-2 + y^2)e^{-\Gamma_1 t} - 2y^2 e^{-(\Gamma_1 + \Gamma_2)t} \right). \quad (20)$$

These witness operators can be measured by four (for the GHZ state) respectively five (for the W state) measurement settings⁴³, compared to the 27 measurement settings required for full state tomography. For the three-qubit GHZ-state, it is straightforward to see from Eq. (19) that the filtered witness is smaller than zero for any finite time, when y is chosen large enough (since its highest power is negative). For the W-state, however, this is not true: the term with y^2 has the prefactor $\exp[-\Gamma_1 t](1 - 2\exp[-\Gamma_2 t])$, which is positive for large t . As a result, using the filtered witness operator instead of

but, interestingly, these two states cannot (not even stochastically) be transformed into each other, and are therefore representatives of different entanglement classes.

Let us now investigate the lifetime of these two states using our decoherence model. After calculating the time evolution of the two states, we obtain for the corresponding fidelities:

$$F_{GHZ}(t) = \frac{1}{4} \left(\exp[-2\Gamma_1 t] + \exp[-\Gamma_1 t] + 2 \exp\left[-\frac{3}{2}(\Gamma_1 + \Gamma_2)t\right] \right), \quad (17)$$

$$F_W(t) = \frac{1}{3} \left(\exp[-\Gamma_1 t] + 2 \exp[-(\Gamma_1 + \Gamma_2)t] \right) \quad (18)$$

From these fidelities, the expectation values of the witnesses can directly be determined as $\langle \mathcal{W}_G \rangle_{\rho_G(t)} = 1/2 - F_{GHZ}(t)$ for the GHZ state, and $\langle \mathcal{W}_W \rangle_{\rho_W(t)} = 2/3 - F_W(t)$ for the W state.

Our next step is to apply the filter operators to the witnesses. This yields the following values for the expectation value of the filtered witness operators:

the unfiltered one does not improve the available detection time. In principle, the witness for the W state can be improved by taking the projector onto the subspace with at most two excitations¹⁸, $\mathbb{1}_2 = \mathbb{1} - |111\rangle\langle 111|$ instead of $\mathbb{1}$. However, in the present case this does not give any improvement, since the $|111\rangle\langle 111|$ state is not populated. The time evolution of the witness expectation values (19) and (20) are plotted in Fig. 2 (for $\Gamma_1 = 10^3 \text{ s}^{-1}$ and $\Gamma_2 = 10^6 \text{ s}^{-1}$).

V. FOUR QUBITS

The more qubits are added, the more distinct classes of entangled states arise. For four qubits, we investigate the following four classes:

$$|GHZ_4\rangle = \frac{1}{\sqrt{2}}(|0101\rangle + |1010\rangle), \quad (21)$$

$$|C_4\rangle = \frac{1}{2}(|0101\rangle + |0110\rangle + |1001\rangle - |1010\rangle), \quad (22)$$

$$|W_4\rangle = \frac{1}{2}(|1000\rangle + |0100\rangle + |0010\rangle + |0001\rangle), \quad (23)$$

$$|D_4\rangle = \frac{1}{\sqrt{6}}(|0011\rangle + |0101\rangle + |0110\rangle + |1001\rangle + |1010\rangle + |1100\rangle). \quad (24)$$

All of these states have been realized in various experiments for different physical systems⁴⁸, but so far not in solid-state nanosystems. Also, some of their decoherence properties have been investigated from different theoretical perspectives^{39,49,50}. The states $|GHZ_4\rangle$ and $|W_4\rangle$ are the four-qubit versions of the states we have investigated for three qubits in the previous section. $|C_4\rangle$ is a representative of the so-called cluster class⁵¹, important in the context of one-way quantum computing⁵². The Dicke state⁵³ $|D_4\rangle$ is an extension of the W-state and consists of all possible permutations of states containing 2 excitations. The fidelity of these states evolves as:

$$F_{GHZ_4}(t) = \frac{1}{2}(\exp[-2\Gamma_1 t] + \exp[-2(\Gamma_1 + \Gamma_2)t]), \quad (25)$$

$$F_{C_4}(t) = \frac{1}{2}(\exp[-2\Gamma_1 t] + \exp[-2(\Gamma_1 + \Gamma_2)t] + \exp[-(2\Gamma_1 + \Gamma_2)t]), \quad (26)$$

$$F_{W_4}(t) = \frac{1}{4}(\exp[-\Gamma_1 t] + 3\exp[-(\Gamma_1 + \Gamma_2)t]), \quad (27)$$

$$F_{D_4}(t) = \frac{1}{6}(\exp[-2\Gamma_1 t] + \exp[-2(\Gamma_1 + \Gamma_2)t] + 4\exp[-(2\Gamma_1 + \Gamma_2)t]). \quad (28)$$

The corresponding projective witnesses can be found, as before, using $c\mathbb{1} - F(t)$, with $c = 1/2$ for the cluster and GHZ-states, $c = 3/4$ for the W-state, and $c = 2/3$ for the Dicke state⁵⁴.

Again, filter operations can be applied in order to prolong the available detection time. The resulting formulas are lengthy and therefore not given here. However, numerically one can directly check that the filter extends the detection time of the GHZ-state to, in principle, infinity. For the other states the situation is different: there the expectation values of the witness operators always become non-negative after some time. However, it is interesting to compare the differences in the evolution of the expectation values of these witness operators for the four classes, and to see which one is the most stable, *i.e.* detectable for the longest time. This is done in Fig. 3.

At this point the same question is arising as for the two-qubit state that we investigated in Sec. III: how does the available detection time depend on the exact state chosen as representative of a class? Or, equivalently, the fidelity of which state decoheres most slowly? In fact, writing the states above in a different basis leads to different decay rates.

This is illustrated in Fig. 4, where the evolution of the witness expectation value of four different cluster states is plotted: $|C_4\rangle$ from Eq. (22), $|C_4^{(16)}\rangle$ is the original cluster state from Ref.⁵⁵ containing 16 terms, and the two additional representations

$$|C_4^{(4)}\rangle = \frac{1}{2}(|0000\rangle + |0011\rangle + |1110\rangle + |1101\rangle), \quad (29)$$

$$|C_4^{(8)}\rangle = \frac{1}{2^{3/2}}(|0000\rangle + |0011\rangle + |0100\rangle + |0111\rangle - |1000\rangle - |1010\rangle + |1101\rangle + |1110\rangle), \quad (30)$$

with 4 and 8 terms, respectively (the first one is a representation with the minimal number of terms, which will be used again in the next section, the second one a rotated version of the original cluster state). As can be seen in Fig. 4, the detection time decreases as the number of terms increases, though the effect is not very large for four and more terms. The representations with the minimal number of terms decohere more slowly. This is not surprising, since for a similar decoherence model one can prove that states with the minimal number of terms are most robust⁴⁹. For representations with the same number of terms, the number of excitations in each term can influence the detectability: which one of the two is easier to detect then depends on the ratio of Γ_1 and Γ_2 .

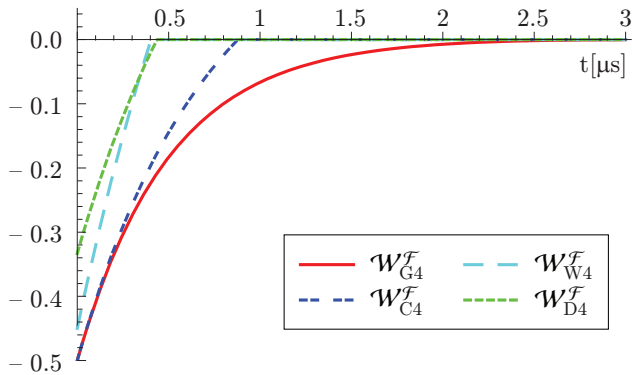


FIG. 3: Expectation values for the filtered witness operators for the four considered classes of fourpartite entangled states (GHZ, cluster, W and Dicke). The filter operator makes the entanglement in the GHZ-state detectable for arbitrarily long times (at least in principle). The entanglement of the other three classes decays faster, but the cluster state is more stable (decays slower) than both the W- and the Dicke states. Parameters used are the same as in Fig. 2.

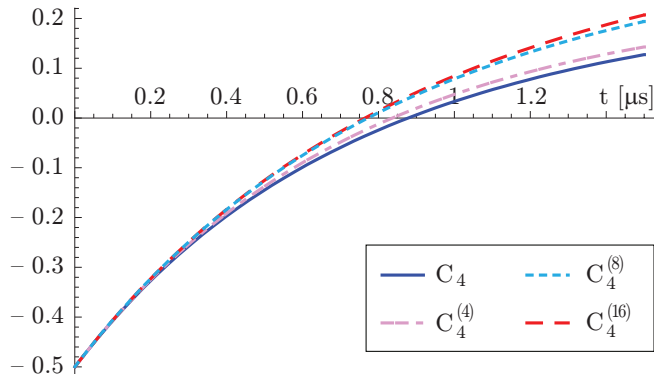


FIG. 4: Expectation values of the witnesses for some fourpartite cluster states. The upper index indicates the number of terms in the representation of each state, the state without index is the one given in Eq. (22). Parameters used are the same as in Fig. 2.

VI. N QUBITS

Let us now consider N qubits. We concentrate on three types of entangled states: GHZ-, W-, and cluster states. For these, there exist proposals how to generate them using available single- and two-qubit operations in quantum dots⁵⁶. Our goal is to calculate the time evolution of the normal (unfiltered) witness for arbitrary N and compare this with the time necessary to generate and measure the state. The representatives of the first two classes can be

written down straightforwardly (for even N):

$$|GHZ_N\rangle = \frac{1}{\sqrt{2}} (|01\dots 01\rangle + |10\dots 10\rangle), \quad (31)$$

$$|W_N\rangle = \frac{1}{\sqrt{N}} (|00\dots 01\rangle + |00\dots 10\rangle + \dots + |10\dots 00\rangle). \quad (32)$$

Calculating the expectation value of the witness operators leads to (for even N):

$$\langle \mathcal{W}_G \rangle_{e_G(t)} = \frac{1}{2} \left(1 - \exp\left[-\frac{N}{2}\Gamma_1 t\right] - \exp\left[-\frac{N}{2}(\Gamma_1 + \Gamma_2)t\right] \right),$$

$$\langle \mathcal{W}_W \rangle_{e_W(t)} = \frac{1}{N} \left(N - 1 - \exp[-\Gamma_1 t] - (N - 1)\exp[-(\Gamma_1 + \Gamma_2)t] \right) \quad (33)$$

The general form of the cluster state – the one we consider here containing the minimal number of terms, namely $2^{N/2}$ – is more complicated; it can be written as⁵⁷

$$|C_N\rangle = \bigotimes_{k=1}^n \frac{[|00\rangle + |11\rangle(\sigma_x \otimes \mathbb{1})]}{\sqrt{2}}, \quad (34)$$

where this formula should be understood as an iteration, with the operator $(\sigma_x \otimes \mathbb{1})$ acting on the Bell state of the next two qubits. For four qubits, this results exactly in the representation $|C_4^{(4)}\rangle$ from Eq. (29), the evolution of which is plotted in Fig. 4.

To calculate the time evolution of the fidelity, we represent the cluster state as⁵²

$$|C_N\rangle \langle C_N| = \prod_{k=1}^N \frac{\mathbb{1} + S_k}{2} \quad (35)$$

with S_k a product of Pauli matrices. We incorporate the effects of dephasing (disregarding the relaxation of the qubits, i.e. setting $\Gamma_1 = 0$, which leads to an error of less than 0.01% for four qubits) in every term in the sum (35). The resulting fidelity of the cluster state can then easily be calculated numerically up to $N = 24$ qubits.

Fig. 5 shows the time at which the expectation value of the (unfiltered) projective witness for each of the three states (33) and (35) becomes positive as a function of the qubit number N , as well as an estimate of the time necessary to generate and measure these states. For electron spin qubits in quantum dots the generation times are taken from Ref.⁵⁶: for both the cluster and the W-states the time required to produce these states is independent of the number of qubits, whereas the production time of states of the GHZ-class scales linearly with the number of qubits. The measurement times are composed as follows: measurement distinguishes between spin-up and spin-down (defined along the z-axis³³) and measuring the components σ_x and σ_y then requires a rotation of the

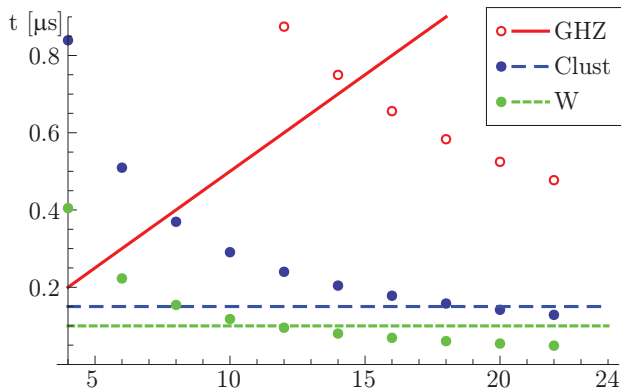


FIG. 5: The dots show the time at which the expectation value of the (unfiltered) witness for a given class of states becomes positive as a function of the qubit number N . Parameters used are $\Gamma_1 = 10^3 s^{-1}$ and $\Gamma_2 = 10^6 s^{-1}$, except for the cluster state where the relaxation is disregarded ($\Gamma_1 = 0$). Also plotted are (shown by lines) the times required to generate the given entangled states, see the text for explanation.

spins by $\pi/2$, which takes about $\sim 50 ns^{58}$. The sum of the generation and the measurement time is given by the lines in the plot.

We see that, as in Figs. 2 and 3, the entanglement of the GHZ-state can be detected for the longest times, but it is more time-consuming to generate than the other two entangled states. Generation and detection of GHZ states should be possible for up to 14 qubits (with the standard projective witness and assuming current operation and decoherence times in quantum dots). The cluster state is the state which can be detected for the largest number of qubits (18), although for up to 12 qubits the “time reserve” (i.e. the difference between the time needed for generation and measurement and the time when the expectation value of the witness operator becomes positive) for the GHZ state is bigger than for

the cluster state. Entanglement of the W-state can be detected for up to 10 qubits.

Finally, it should be noted that the N -qubit GHZ state can, in principle, be detected for all times when using the filter technique for the analysis of the measurement results. This follows from similar arguments as for the two- and three-qubit case.

VII. CONCLUSION

In conclusion, we have investigated entanglement and its detectability in a linear array of qubits which locally undergo decoherence modeled by two decay rates: Γ_1 for relaxation and Γ_2 for dephasing. We have discussed in detail the cases of two, three and four qubits, and we compared different classes of entangled states with each other, namely the GHZ-, W-, cluster and Dicke classes of entangled states. Using witness operators as detectors of entanglement and introducing a new class of these operators, the filtered witnesses, we estimated the maximum available detection time for these types of entangled states. We also gave limits on the maximum number of entangled qubits that can be created and measured based on currently known decoherence times for electron spin qubits in quantum dots. The most suitable entangled state turns out to be the GHZ-state, which is, at least in principle, entangled for any number of qubits at any finite time. Our results can help to make a choice as to which state to prepare in experiments. Since local decoherence is characteristic for many types of solid-state qubits, our model and the filtered operator technique are applicable to a variety of these qubits.

This work has been supported by The Netherlands Organisation for Scientific Research (NWO), the FWF (START prize) and the EU (SCALA, OLAQUI, QICS).

¹ A. Einstein, B. Podolski, and N. Rosen, Phys. Rev. Lett. **47**, 777 (1935).

² E. Schrödinger, Naturwissenschaften **23**, 807 (1935).

³ J. S. Bell, Physics **1**, 195 (1964).

⁴ R. F. Werner, Phys. Rev. A **40**, 4277 (1989).

⁵ R. Horodecki, P. Horodecki, M. Horodecki, and K. Horodecki, arXiv:quant-ph/0702225.

⁶ M. A. Nielsen and I. L. Chuang, *Quantum Computation and Quantum Information*, (Cambridge University Press, Cambridge, UK, 2000).

⁷ R. Hanson, L. P. Kouwenhoven, J. R. Petta, S. Tarucha, and L. M. K. Vandersypen, Rev. Mod. Phys. **79**, 1217 (2007).

⁸ G. Wendin and V. S. Shumeiko, in the *Handbook of Theoretical and Computational Nanotechnology*, **1**, 129; see also arXiv:cond-mat/0508729.

⁹ For a recent overview of more solid-state qubit systems such as *e.g.* nitrogen-vacancy centers in diamond, see R.

Hanson and D. D. Awschalom, Nature **453**, 1043 (2008) and references therein.

¹⁰ See *e.g.* H.-A. Engel and D. Loss, Phys. Rev. B **65**, 195321 (2002).

¹¹ M. Horodecki, P. Horodecki, and R. Horodecki, Phys. Lett. A **223**, 1 (1996).

¹² B. M. Terhal, Phys. Lett. A **271**, 319 (2000).

¹³ M. Lewenstein, B. Kraus, J. I. Cirac, and P. Horodecki, Phys. Rev. A **62**, 052310 (2000); B. M. Terhal, Phys. Lett. A **271**, 319 (2000).

¹⁴ O. Gühne, P. Hyllus, D. Bruß, A. Ekert, M. Lewenstein, C. Macchiavello, and A. Sanpera, Phys. Rev. A **66**, 062305 (2002).

¹⁵ O. Gühne, P. Hyllus, D. Bruss, A. Ekert, M. Lewenstein, C. Macchiavello, and A. Sanpera, J. Mod. Opt. **50**, 1079 (2003).

¹⁶ M. Bourennane, M. Eibl, C. Kurtsiefer, S. Gaertner, H. Weinfurter, O. Gühne, P. Hyllus, D. Bruß, M. Lewenstein,

- and A. Sanpera, Phys. Rev. Lett. **92**, 087902 (2004).
- ¹⁷ C.-Y. Lu, X.-Q. Zhou, O. Gühne, W.-B. Gao, J. Zhang, Z.-S. Yuan, A. Goebel, T. Yang, and J.-W. Pan, Nature Physics **3**, 91 (2007).
- ¹⁸ D. Leibfried *et al.*, Nature **438**, 639 (2005); H. Häffner *et al.*, Nature **438**, 643 (2005).
- ¹⁹ M. Blaauboer and D. P. DiVincenzo, Phys. Rev. Lett. **95**, 160402 (2005); L. Faoro and F. Taddei, Phys. Rev. B **75**, 165327 (2007).
- ²⁰ M. Schlosshauer, Rev. Mod. Phys. **76**, 1267 (2005).
- ²¹ D. Loss and D. P. DiVincenzo, Phys. Rev. A **57**, 120 (1998).
- ²² G. Dresselhaus, Phys. Rev. **100**, 580 (1955).
- ²³ E. I. Rashba, Sov. Phys. Solid State **2**, 1109 (1960) [Fiz. Tverd. Tela **2**, 1109 (1960)].
- ²⁴ A. V. Khaetskii and Yu. V. Nazarov, Phys. Rev. B **61**, 12639 (2000).
- ²⁵ A. V. Khaetskii and Yu. V. Nazarov, Phys. Rev. B **64**, 125316 (2001).
- ²⁶ V. N. Golovach, A. Khaetskii, and D. Loss, Phys. Rev. Lett. **93**, 016601 (2004).
- ²⁷ A. Abragam, *The Principles of Nuclear Magnetism*, (Oxford University Press, 1961).
- ²⁸ D. Paget, G. Lampel, B. Sapoval, and V. I. Safarov, Phys. Rev. B **15**, 5780 (1977).
- ²⁹ A. V. Khaetskii, D. Loss, and L. Glazman, Phys. Rev. Lett. **88**, 186802 (2002).
- ³⁰ I. A. Merkulov, A. L. Efros, and M. Rosen, Phys. Rev. B **65**, 205309 (2002);
- ³¹ P.-F. Braun *et al.*, Phys. Rev. Lett. **94**, 116601 (2005); A. C. Johnson, J. R. Petta, J. M. Taylor, A. Yacoby, M. D. Lukin, C. M. Marcus, M. P. Hanson, and A. C. Gossard, Nature **435**, 925 (2005); F. H. L. Koppens, J. A. Folk, J. M. Elzerman, R. Hanson, L. H. Willems van Beveren, I. T. Vink, H. P. Tranitz, W. Wegscheider, L. P. Kouwenhoven, L. M. K. Vandersypen, Science **309**, 1346 (2005).
- ³² R. Hanson, B. Witkamp, L. M. K. Vandersypen, L. H. Willems van Beveren, J. M. Elzerman, and L. P. Kouwenhoven, Phys. Rev. Lett. **91**, 196802 (2003).
- ³³ J. M. Elzerman, R. Hanson, L. H. Willems van Beveren, B. Witkamp, L. M. K. Vandersypen, and L. P. Kouwenhoven, Nature **430**, 431 (2004).
- ³⁴ R. G. Shulman, B. J. Wyluda, and H. J. Hrostowski, Phys. Rev. **109**, 808 (1958).
- ³⁵ This is not confirmed experimentally, but the very slow decay of nuclear spin polarization of up to several minutes is an indication for slow change of B_{nuc}^z ; see *e.g.* A. K. Hüttel, J. Weber, A. W. Holleitner, D. Weinmann, K. Eberl, and R. H. Blick, Phys. Rev. B **69**, 073302 (2004).
- ³⁶ J. M. Kikkawa and D. D. Awschalom, Phys. Rev. Lett. **80**, 4313 (1998).
- ³⁷ B. Herzog and E. L. Hahn, Phys. Rev. **103**, 148 (1956).
- ³⁸ G. Lindblad, Commun. Math. Phys. **48**, 119 (1976).
- ³⁹ A. R. R. Carvalho, F. Mintert, and A. Buchleitner, Phys. Rev. Lett. **93**, 230501 (2004).
- ⁴⁰ F. G. S. L. Brandão, Phys. Rev. A **72**, 022310 (2005); D. Cavalcanti and M. O. Terra Cunha, Appl. Phys. Lett. **89**, 084102 (2006); O. Gühne, M. Reimpell, and R. F. Werner, Phys. Rev. Lett. **98**, 110502 (2007); J. Eisert, F. Brandão, and K. Audenaert, New J. Phys. **9**, 46 (2007).
- ⁴¹ A. Peres, Phys. Rev. Lett. **77**, 1413 (1996); M. Horodecki, P. Horodecki, and R. Horodecki, Physics Letters A **223**, 1 (1996).
- ⁴² Using another witness based on stabilizers we can even reduce the number of measurement settings to two; this witness can be decomposed as
- $$\mathcal{W}_{stab} = \frac{y^2}{2}\sigma_x \otimes \sigma_x + \frac{1+y^4}{4}(\mathbb{1} \otimes \mathbb{1} + \sigma_z \otimes \sigma_z) + \frac{1-y^4}{4}(\sigma_z \otimes \mathbb{1} + \mathbb{1} \otimes \sigma_z). \quad (36)$$
- \mathcal{W}_{stab} is a little less robust against noise, but two local measurements are the least possible. See also G. Tóth and O. Gühne, Phys. Rev. Lett. **94**, 060501 (2005).
- ⁴³ O. Gühne and P. Hyllus, Int. J. Theor. Phys. **42**, 1001 (2003).
- ⁴⁴ W. Dür, G. Vidal, and J. I. Cirac, Phys. Rev. A **62**, 062314 (2000).
- ⁴⁵ A. Acín, D. Bruß, M. Lewenstein, and A. Sanpera, Phys. Rev. Lett. **87**, 040401 (2001).
- ⁴⁶ Daniel M. Greenberger, Michael A. Horne, Anton Zeilinger: *Bell's theorem, Quantum Theory, and Conceptions of the Universe*, pp. 73-76, (Kluwer Academic, Dordrecht, The Netherlands, 1989), see also arXiv:0712.0921; D. M. Greenberger, M. A. Horne, A. Shimony, and A. Zeilinger, Amer. J. Phys. **58**, 1131-43 (1990).
- ⁴⁷ F. Verstraete, J. Dehaene, B. De Moor, and H. Verschelde, Phys. Rev. A **65**, 052112 (2002); L. Lamata, J. León, D. Salgado, and E. Solano, Phys. Rev. A **75**, 022318 (2007).
- ⁴⁸ See *e.g.* Refs.^{16,17} and¹⁸ for realizations of GHZ, W, and cluster states of up to 8 qubits using photons and ions, respectively, and N. Kiesel, C. Schmid, G. Tóth, E. Solano, and H. Weinfurter, Phys. Rev. Lett. **98**, 063604 (2007) for a four-qubit Dicke photon state.
- ⁴⁹ O. Gühne, F. Bodoky, and M. Blaauboer, arXiv:0805.2873.
- ⁵⁰ C. Simon and J. Kempe, Phys. Rev. A **65**, 052327 (2002); W. Dür and H.J. Briegel, Phys. Rev. Lett. **92**, 180403 (2004); L. Aolita, R. Chaves, D. Cavalcanti, A. Acín, and L. Davidovich, Phys. Rev. Lett. **100**, 080501 (2008); A. Borrás, A. P. Majtey, A. R. Plastino, M. Casas, and A. Plastino, arXiv:0806.0779.
- ⁵¹ R. Raussendorf and H.-J. Briegel, Phys. Rev. Lett. **86**, 5188 (2001).
- ⁵² M. Hein, W. Dür, J. Eisert, R. Raussendorf, M. Van den Nest, and H.-J. Briegel: in *Proceedings of the International School of Physics Enrico Fermi on Quantum Computers, Algorithms and Chaos*, (Varenna, Italy, 2005); see also arXiv:quant-ph/0602096.
- ⁵³ R. H. Dicke, Phys. Rev. **93**, 99 (1954).
- ⁵⁴ G. Tóth, J. Opt. Soc. Am. B **24**, 275 (2007).
- ⁵⁵ See Eq. (2) in H.-J. Briegel and R. Raussendorf, Phys. Rev. Lett. **86**, 910 (2001).
- ⁵⁶ F. Bodoky and M. Blaauboer, Phys. Rev. A **76**, 052309 (2007).
- ⁵⁷ In general, a cluster state is defined as an eigenstate of certain local observables^{51,52}; here we choose them as $\mathcal{S}_1 = \sigma_z \sigma_z \mathbb{1} \dots$; $\mathcal{S}_2 = \sigma_x \sigma_x \sigma_x \mathbb{1} \dots$; $\mathcal{S}_3 = \mathbb{1} \sigma_z \sigma_z \sigma_z \mathbb{1} \dots$; \dots ; $\mathcal{S}_N = \mathbb{1} \dots \mathbb{1} \sigma_x \sigma_x$. This is locally equivalent to the definition as in^{51,52}; however, the state given in Eq. (34) contains the minimal number of terms; see Ref.⁴⁹.
- ⁵⁸ F. H. L. Koppens, C. Buizert, K. J. Tielrooij, I. T. Vink, K. C. Nowack, T. Meunier, L. P. Kouwenhoven, and L. M. K. Vandersypen, Nature **442**, 766 (2006).